CrossMark

In situ Raman imaging of high-temperature solid-state reactions in the CaSO$_4$–SiO$_2$ system

Nadine Böhme[1] · Kerstin Hauke[1] · Manuela Neuroth[2] · Thorsten Geisler[1]

Abstract The deposition of mineral phases on the heat transfer surfaces of brown coal power plants may have a negative effect on power plant boilers. The paragenesis of these deposits contains information about the actual temperature prevailed during the combustion of lignite, if the temperature-dependences of distinct mineral transformations or reactions are known. Here, we report results of a sintering study (to ∼ 1100 °C) with samples containing anhydrite, quartz, and gehlenite, which are typical components of Rhenish lignite ashes. Thermal decompositions and solid-state reactions were analyzed (1) in situ and (2) both in situ and after quenching using confocal hyperspectral Raman imaging. This novel application of confocal Raman spectroscopy provides temperature- and time-resolved, 2-dimensional information about sintering processes with a micrometer-scale resolution. In the course of the sintering experiments with anhydrite and quartz with a weight ratio of 2:1 both polymorphs wollastonite and pseudowollastonite were identified in situ at about 920 and 1000 °C, respectively. The formation of pseudowollastonite was thus observed about 120 °C below the phase transition temperature, demonstrating that it can form metastably. In addition, α'_L-Ca$_2$SiO$_4$ was identified at about 1100 °C. In samples containing equal weight fractions of anhydrite and quartz that were quenched after firing for 9 h at about 1100 °C, β-Ca$_2$SiO$_4$ (larnite) crystallized as rims around anhydrite grains and in direct contact to wollastonite. We furthermore observed that, depending on the ratio between quartz and anhydrite, wollastonite replaced quartz grains between 920 and 1100 °C., i.e., the higher the quartz content, the lower the formation temperature of wollastonite.

Keywords Ash deposition · Calcium silicate · Calcium sulfate · High-temperature · Raman imaging

1 Introduction

During the combustion process of lignite in a brown coal power plant, the deposition of mineral phases on the heat transfer surfaces may have a negative effect on power plant boilers. Such ash deposition, including fouling and slagging, can reduce the heat conductibility and consequently the efficiency of the power station. The temperature at which sintering reactions take place strongly depends on coal composition. Therefore, it is important to determine the mineralogical composition of brown coal before firing it. Furthermore, it is of great interest to understand the mechanism of ash transformation of different coals worldwide (Nankervis and Furlong 1980; Vuthaluru and Zhang 2001; Kostakis 2011; Li et al. 2016, 2017). Currently, there exists a wide range of analytical techniques to classify varieties of brown coals according to its combustion behavior, such as X-ray fluorescence (XRF), scanning electron microscopy (SEM), and X-ray diffraction (XRD). These methods have also frequently been applied to study mineral reactions associated with the burn up of brown coals (e.g., Nankervis and Furlong 1980; Li et al.

✉ Nadine Böhme
  nadine.boehme@uni-bonn.de

1 Institut für Geowissenschaften und Meteorologie, Universität Bonn, Poppelsdorfer Schloss, Meckenheimer Allee 169, 53115 Bonn, Germany

2 RWE Power AG, F und E, Kraftwerk Niederaußem, Bergheim, Germany

2016, 2017) as well as with natural lignite combustion deposits (Kostakis 2011).

Anhydrite, quartz, and gehlenite are typical components of Rhenish brown coal ashes. Sintering reactions between these phases at high temperature may lead to adherent soiling and poorly removable sintering crusts inside the boiler of power stations. Anhydrite has, in combination with sodium sulfate, adhesive properties and supports ash deposition (Kostakis 2011; Li et al. 2016). Li et al. (2016, 2017) have studied ash depositions formed on an air-cooled probe and pointed out that early deposits consist of fine Ca/S particles that connect coarser fragments and initiate ash accumulation. On the other hand, CaO helps to capture gaseous SO_2/SO_3 (Li et al. 2017). Anhydrite is the main sulfur-containing mineral phase in the solid combustion waste from 500 °C until its decomposition temperature of about 1200 °C (e.g., Hofman and Mostowitsch 1909) and the main crystalline phase involved in the sulfur retention in the combustion waste. A considerable proportion of SO_2/SO_3 would not be emitted into the flue gas at firing temperatures lower than the decomposition temperature of anhydrite. However, the decomposition temperature of anhydrite changes in the presence of other minerals (Mihara et al. 2007). For example, quartz can suppress fouling at low temperatures (Li et al. 2016), but also leads to the formation of calcium silicates at high temperatures when in contact to CaO-bearing minerals. It was found as main component of fouling and slagging deposits (Nankervis and Furlong 1980; Kostakis 2011). Calcium silicates play a major role not only during power plant operation. Wollastonite ($CaSiO_3$) and dicalcium silicates (Ca_2SiO_4) are important minerals for a number of industrial applications. The main applications of wollastonite are in the ceramic and building industry, because of its high melting point, thermal stability, and fluxing characteristics. Due to its acicular structure, wollastonite particularly improves the mechanical properties of building components. Both wollastonite and dicalcium silicate are also cement-relevant phases. For instance, dicalcium silicate is an important ingredient of Portland cement clinker. Other potential applications exist in biomedicine due to its excellent bioactivity (e.g., Mohammadi et al. 2014).

Due to the importance of calcium silicate minerals, numerous sintering experiments with CaO-bearing minerals and quartz have been performed to synthetize wollastonite and dicalcium silicate (e.g., Remy et al. 1997; Rashid et al. 2014). However, none of the experiments, with two exceptions (Stange et al. 2018; Hauke et al. 2019), were carried out in situ as a function of temperature and time. Modern confocal Raman spectrometer systems with integrated heating stages allow the 'visualization' of mineral reactions and textures even at high temperatures with a spatial resolution of a few micrometers (Stange et al.

2018; Hauke et al. 2019). Therefore, it is an exceptional method to in situ follow high-temperature phase transformations and reactions. The advantages of confocal Raman spectroscopy compared to conventional experimental and analytical methods, where the sample has to be quenched to room temperature (RT) before being analyzed, has clearly been demonstrated by Stange et al. (2018). These authors were the first, who have investigated solid–solid reactions in calcite-bearing kaolin during high-temperature sintering by hyperspectral Raman imaging. One important result of their study was that in an in situ experiment calcite decomposition occurred at temperatures below 750 °C, whereas in a quench experiment calcite was still detectable at temperature above 1000 °C, because calcite recrystallized during cooling. A detailed understanding of thermodynamics and kinetics of high-temperature solid-state and melting reactions and thus the mechanism of mineral reactions and transformations is essential to predict sinter reactions in brown coal blocks at a given temperature.

In the present study, samples of anhydrite, gehlenite, and quartz were fired to about 1100 °C and the reactions were analyzed in situ by hyperspectral Raman imaging. The aim was to visualize phase reactions between these minerals and gain kinetic and thermodynamic information about mineral growth and breakdown. In order to use mineral phases as indicators to estimate temperature conditions during the combustion of lignite, it is necessary to understand their reaction behavior at high temperatures. Taking into account all calcium phases that can potentially form during firing, different weight and molar ratios of the raw materials were used for the experiments. Of particular interest was to investigate the formation of wollastonite and dicalcium silicate as a function of the quartz content in the anhydrite-quartz system. The prime questions were: (1) does quartz affect the decomposition behavior of anhydrite, (2) does sulfate promote the crystallization of calcium silicates, (3) does temperature influence the formation of different calcium phases, and (4) does quenching have an effect on the sintering products. Additionally, we aim to demonstrate the power of in situ Raman imaging of high-temperature sintering reactions.

2 Materials and methods

2.1 Sample preparation

To study the influence of composition on the formation temperature of the calcium silicates in the quartz-anhydrite system, several sintering experiments with varying quartz-anhydrite composition ratios were carried out (Table 1). Additionally, gehlenite was added in one experiment to the

Table 1 Experimental conditions

Exp.	Anh:Qtz(:Geh) (wt%)	Type of experiment	T range (°C)	T steps (°C)	T rate (°C/min)	Acquisition time (s)	Dwell time (h)
AQ-1	1:1	in situ	815, 850–1200	50	10 ↗↘	2 × 1	6.5
AQ-2.1	2:1	in situ	500–800, 900–1200	100	10 ↗↘	1 × 0.5	2 × 2 (4)[a]
AQ-2.2	2:1	in situ/quench	900–1200	100	10 ↗↘	1 × 0.5	2 × 2 (4)[a]
AQ-3.1	4.5:1	in situ	950–1250	50	10 ↗↘	1 × 0.5	2 × 2 (4)[a]
AQ-3.2	4.5:1	in situ/quench	900–1200	100	10 ↗; 50 ↘	1 × 0.5	2 × 2 (4)[a]
AQG-1	1:1:1	in situ	450, 900	450	10 ↗↘	1 × 0.5	3 × 2 (6)[a]

[a]During a dwell time of 4 or 6 (AQG-1) h, two respectively three (AQG-1) Raman images with a recording time of about 2 h were recorded

anhydrite-quartz system to study the influence of (1) an additional Ca source and (2) Al added to the system (Table 1: exp. AQG-1). The sample mixtures were prepared from natural crystals of anhydrite, quartz, and gehlenite. These crystals were obtained from the Mineralogical Museum of the University of Bonn, Germany. The anhydrite and gehlenite crystals stem from Tirol, Austria. The origin of the quartz crystal is unknown. Light microscopic images of anhydrite and quartz revealed no contamination of other minerals. The gehlenite, however, was partly overgrown by grossular, which was confirmed by a XRD analysis. The minerals were ground in an agate mortar to obtain different grain sizes between about 20 and 60 μm. Several green bodies were produced by compacting 50 mg of precursor material into cylinders (3 mm × 3 mm) at a pressure of 10 kPa. Before firing, all samples were checked for with the occurrence of initial calcium silicates.

2.2 Raman spectroscopy

The Raman measurements were carried out using a Horiba Scientific HR800 Raman spectrometer equipped with a 2 W Nd:YAG laser (λ = 532.09 nm), an electron-multiplier CCD detector, and an Olympus BX41 microscope. A 50 × long-working distance objective with a numerical aperture (NA) of 0.5, a grating with 600 grooves/mm, and a 100 μm spectrometer entrance slit were used for the measurements. The lateral and axial (depth) resolution of a Raman measurements with the focus at the sample surface is usually estimated from the theoretical diffraction limit given by $d_l \approx 1.22\lambda/NA$ and $d_a \approx 4\lambda/NA^2$, yielding 1.3 and 8.5 μm, respectively. However, these values should be understood as the best resolution theoretically possible. The real lateral and axial resolution may rather be in the

order of $d_l \approx 2$ μm and $d_a \approx 15$ μm, respectively. It is important to note that the axial resolution at the surface also depends on the absorption properties of the material investigated. A Raman intensity loss of 20% to 40% is observed within the first ten micrometers, whereas within the first 20 μm, which is a typical grain diameter, already about half of the intensity of the Raman bands is lost (Hauke et al. 2019). The spectral resolution was 3.5 cm⁻¹, as given by the line width of a Ne line at 1707.062 cm⁻¹ that was recorded as "internal" frequency standard in all spectra. For the sintering experiments, a LINKAM TS 1500 heating stage was mounted on an automated x–y–z stage. Due to the height and the volume of the sample cylinder, a strong temperature gradient occurs within the furnace. This gradient was empirically determined by a procedure that is described in detail in Stange et al. (2018). With this procedure, the corrected temperatures are accurate within ± 5 °C. In the following, the corrected temperatures are given.

In general, in situ hyperspectral Raman images were recorded from an area of 100 μm × 100 μm with a 1 μm step size (100 μm × 100 μm = 10,000 pixel per image) in x and y direction. The individual Raman spectra were collected during continuous x–y stage movement with a speed of 2 μm/s (SWIFT© mode). During movement, Raman intensities were recorded for 0.5 s in the wavenumber range from 100 to 1730 cm⁻¹. The total exposure time was about 2 h for a single image. Two types of Raman experiments were performed to study the effect of quenching the sample to room temperature (RT) before Raman imaging. However, experiments AQ-1 and AQ-2.1 were the first experiments that were performed. These experiments contain a few individual trials to figure out the best experimental conditions for further experiments. The experimental conditions of each experiment are
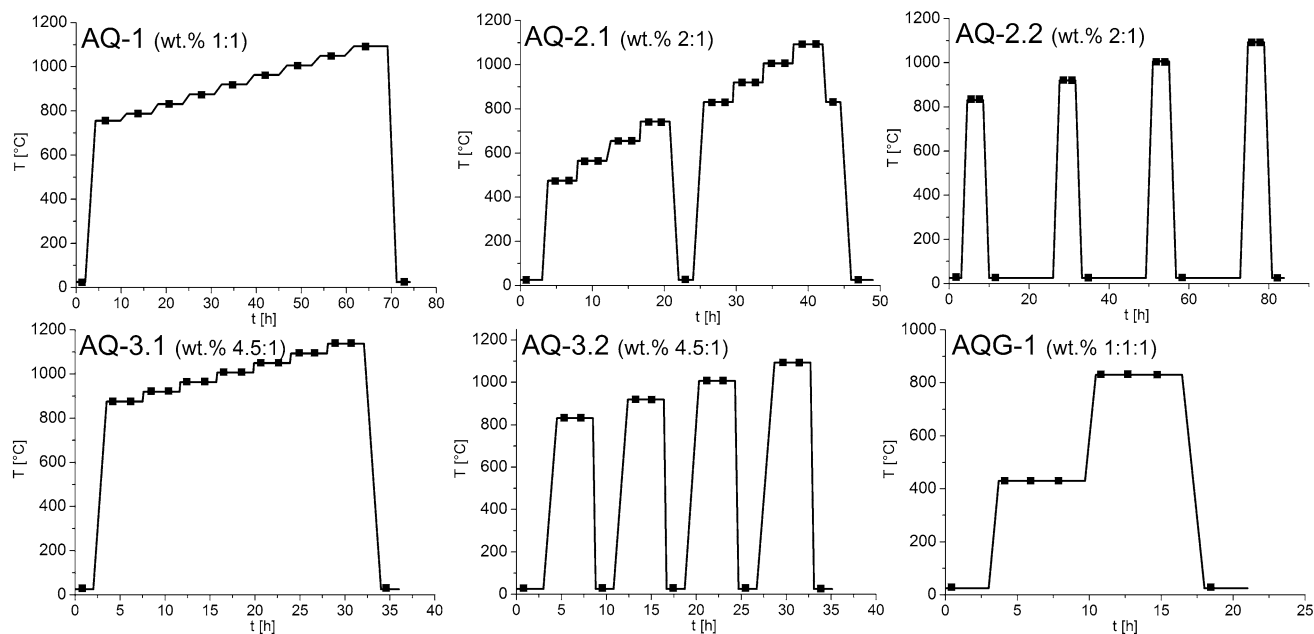
Fig. 1 Temperature histories of the in situ and the in situ/quench experiments. (In the in situ/quench experiments the sample was fired to the sintering temperatures and two hyperspectral Raman images were subsequently recorded. Afterwards the sample was quenched to RT before a last Raman image was recorded. In the in situ experiments, the green bodies were progressively fired to higher temperatures and Raman images were recorded in situ. Squares represent the start of each measurement.)

summarized in Table 1 and the temperature history is illustrated in Fig. 1. In general, at 815 °C lignite is reduced to ash. The first experiment was therefore carried out by firing the sample at 815 ± 5 °C for 2.5 h before a hyperspectral Raman image was recorded with a recording time of about 6.5 h. Afterwards the sample was fired to 850 ± 5 °C and stepwise (50 °C) to 1200 ± 5 °C and finally cooled down to RT. At each temperature step, a Raman image was taken with 2 × 1 s acquisition time for a single pixel of the image. The results of experiment AQ-1 demonstrated that such long single-point acquisition time are not necessary to obtain a sufficient image quality in this system. Therefore, the acquisition time was reduced to 0.5 s per point (pixel) for further experiments. To test whether mineral transformations already take place in the system below about 900 °C, a sample was fired between 500 ± 5 and 800 ± 5 °C in 100 °C-steps and then quenched to RT. Since the images taken in this temperature range revealed no significant mineral changes, further Raman images were recorded above 900 °C only. In the remaining course of experiment AQ-2.1 the sample was fired again to 900 ± 5 °C and further to 1200 ± 5 °C in 100 °C-steps (Fig. 1). At each temperature step a hyperspectral Raman image was recorded. The continuous cooling by 10 °C/min was interrupted at 900 ± 5 °C to record a Raman image. The image revealed no additional information to the images recorded at 1200 ± 5 °C or RT.

Thus, the following experiments were quenched directly to RT before taking a hyperspectral Raman image.

As mentioned above, two types of experiments were carried out. During the first type of experiments (in situ/quench experiments), the green body was fired to high temperatures with a heating rate of 10 °C/min. Immediately after reaching the respective temperature, two in situ hyperspectral Raman images were taken in a row. Thus, the second image was recorded after a dwell time of 2 h. Afterwards the sample was quenched to RT with a cooling rate of 10 °C/min before a RT Raman image was recorded. Then, the sample was fired to the next temperature step until the maximum temperature had been reached (Fig. 1). The analysis of the quenched sample corresponds to a conventional sinter experiment during which the sample has to be quenched to RT before being analyzed. In the second type of experiments, the samples were fired to high temperature without quenching the sample. Two subsequent Raman images were taken at each temperature step before the sample was further heated to the next temperature (Fig. 1). After reaching the final temperature, the sample was cooled down to RT and a final Raman image was recorded.

2.3 Data treatment and analysis

In general, mineral phases are identified by the characteristic positions and relative intensities of their fundamental

Raman bands. With increasing temperature, the Raman bands of mineral phases usually shift to lower wavenumbers and their linewidth (full width of half-maximum) increases (e.g., Stange et al. 2018). Additionally, the black body radiation of the sample increases with increasing temperature and thereby progressively reduces the signal-to-noise ratio. The identification of minerals at high temperatures is complicated by the fact that reference Raman spectral databases, such as, e.g., the RRUFF database (Laetsch and Downs 2006), only contain RT spectra that usually differ significantly from their high-temperature (HT) counterparts. Therefore, we started to collect HT Raman spectra of relevant pure mineral phases, including, e.g., quartz, anhydrite, wollastonite, and pseudowollastonite, in order to identify mineral phases in multi-component systems but also for the quantitative phase determination (see below).

The data reduction and creation of hyperspectral false color Raman images was carried out using the LabSpec 6 program. The images show the 2-dimensional, micrometer-scale distribution of mineral phases at a given temperature. The dominant mineral phase in a given Raman spectrum was determined by the classical least-squares (CLS) fitting procedure. This mathematical procedure is based on the assumption that a multiphase spectrum is a simple mixture of spectra of each individual phase (Fig. 2). Mixed spectra are unavoidable due to the limitation in the lateral and, in particular, the depth resolution with respect to the grain sizes. At each point within the multidimensional spectral field, the CLS matching procedure finds a linear combination of reference spectra from the pure phases that best describe the respective raw spectrum. Our own temperature-depend Raman spectra, recorded under the same experimental conditions, were used as input spectra in the CLS fitting procedure to obtain the relative phase proportions, as described in more detail in Stange et al. (2018) and Hauke et al. (2019). This procedure, at least partly, takes into account differences in the Raman cross sections (Hauke et al. 2019). Eventually, the image is generated by coloring each pixel (point) relative to the proportion of individual components in the spectrum. As an example, Fig. 3 shows the HT Raman spectra of anhydrite, quartz, and wollastonite collected at 1090 ± 5 °C, which were used to analyze the image recorded at 1093 ± 5 °C. The false-colored hyperspectral Raman images are presented in the unmixed mode that displays the phase with the highest fractional intensity within a Raman spectrum with a color assigned to that phase (Stange et al. 2018; Hauke et al. 2019). The color shading of a pixel from bright to dark further renders the total fraction of that phase, with bright and dark coding reflecting higher and lower fractions, respectively.

In Fig. 2, creation of a false-color image with the classical least-squares (CLS) fitting method using high-temperature reference spectra of pure phases, collected under the same experimental conditions. This mathematical method is based on the assumption that a multiphase spectrum is a simple mixture of the spectra of each individual phase, here quartz and anhydrite. Quartz (red) is identifiable by its most intense Raman band near 464 cm^{-1} and anhydrite (blue) by the intense $\nu_1(SO_4)$ band near 1015 cm^{-1}.

In Fig. 3, High-temperature (1090 ± 5°) reference Raman spectra of wollastonite, anhydrite, and quartz which were used to generate the hyperspectral Raman image shown in the lower right corner (from exp. AQ-3.1). (Note that each mineral phase can clearly be identified by its characteristic Raman spectrum.)
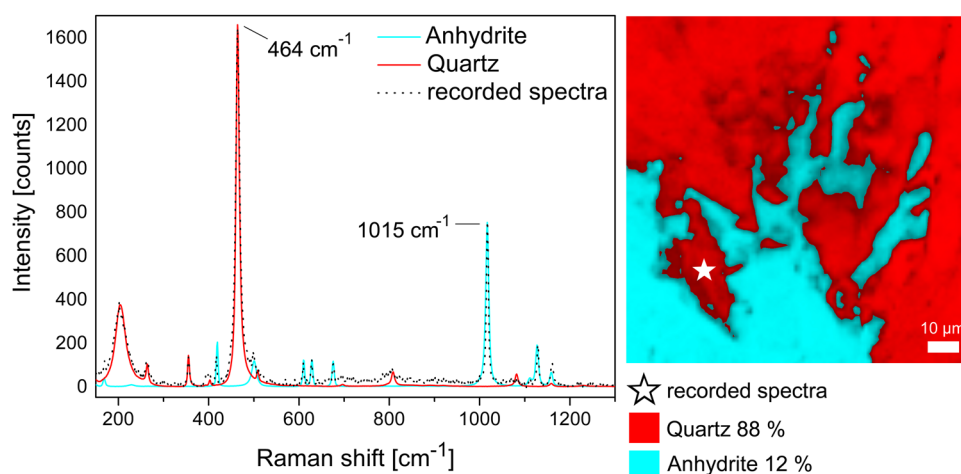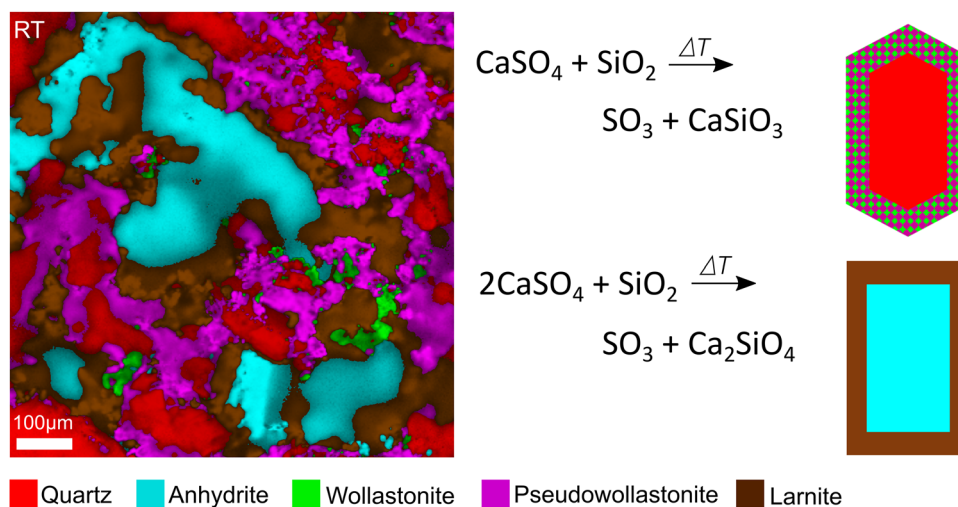

Fig. 2 A false-color image
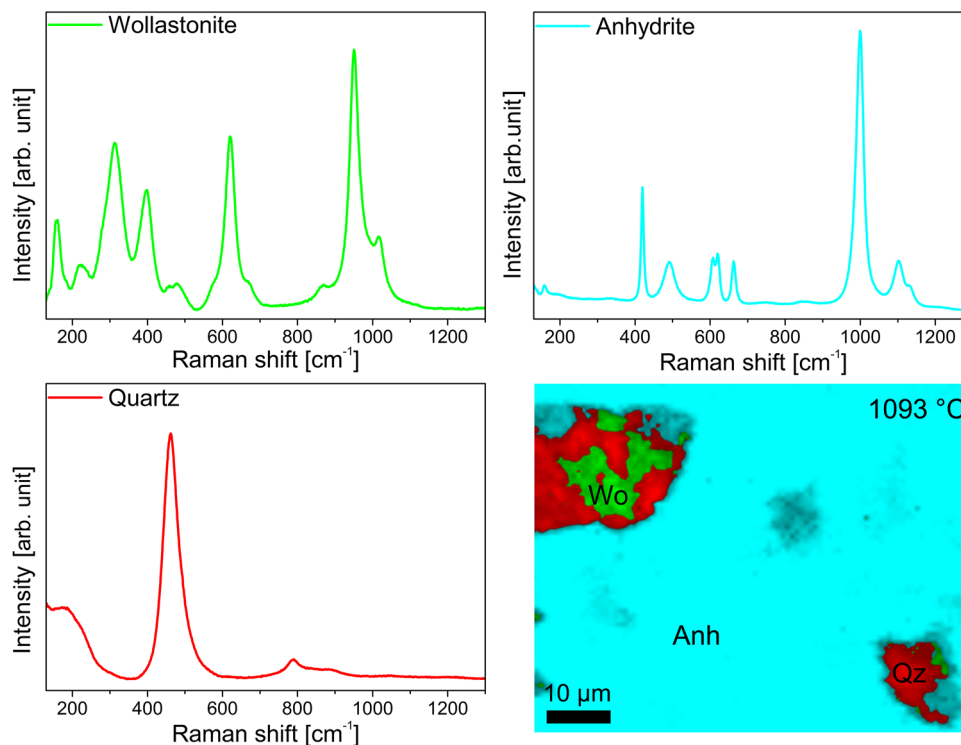
Fig. 3 High-temperature (1090 ± 5 °) reference Raman spectra of wollastonite, anhydrite, and quartz

Fig. 4 Normalized false-color hyperspectral Raman images of the in situ experiment AQ-1

3 Results

3.1 In situ experiment AQ-1 (Anh + Qz, wt% 1:1)

Normalized false-color hyperspectral Raman images (not shown here) collected during experiment AQ-1 (Fig. 1a) displays no reaction between anhydrite and quartz within the imaged area up to a temperature of 1093 ± 5 °C.

Surprisingly, only after the sample had been cooled down to RT after a total sintering time of 9 h at 1093 ± 5 °C, wollastonite, pseudowollastonite, and the dicalcium silicate larnite were identified as reaction products (Fig. 4). At RT, wollastonite and its high-temperature polymorph pseudowollastonite had formed rims around quartz grains, whereas larnite is located in contact to anhydrite or pseudowollastonite grains. It follows that the new phases must

have crystallized during cooling, since they could not be identified in situ at high temperatures.

In Fig. 4, after 9 h sintering at 1093 ± 5 °C the sample was quenched to RT. Wollastonite and pseudowollastonite crystallized around quartz grains and larnite could be identified as rims around anhydrite and near to pseudowollastonite grains. The two reactions leading to a monocalcium silicate rim around quartz and a dicalcium silicate rim around anhydrite are also given.

3.2 In situ experiment AQ-2.1 and in situ/quench experiment AQ-2.2 (Anh + Qz, wt% 2:1)

The solid-state reactions during experiments AQ-2.1 and AQ-2.2 (higher anhydrite content as AQ-1) were investigated by Raman spectroscopy at sintering-temperatures of up to 1093 ± 5 °C. In exp. AQ-2.1 the 100 μm × 100 μm-sized images were recorded at each temperature step before the sample was fired to the next temperature step (Fig. 1b). Unless otherwise described, there is no change in mineral content at lower temperatures and increasing dwell time. In experiment AQ-2.2 the sample was analyzed at each temperature step and after quenching before firing to the next temperature step (Fig. 1c). From Fig. 5 it is discernable that wollastonite started to crystallize at 919 ± 5 °C while the first image was recorded. With increasing reaction time, more and more wollastonite crystallized by mainly replacing anhydrite. After 2 h at 1093 ± 5 °C rims of wollastonite have formed along anhydrite-quartz interfaces. Furthermore, at this temperature, a new phase with an intense Raman band near 843 cm^{-1} was identified in direct contact to wollastonite. After quenching to RT, larnite could be identified at the same location. Obviously, the high temperature modification of dicalcium silicate α'_L-Ca₂SiO₄ must have formed at 1093 ± 5 °C (Fig. 5). The hyperspectral Raman images of the in situ/quench experiment (AQ-2.2) show that wollastonite crystallized at 919 ± 5 °C at grain boundaries between anhydrite and quartz (Fig. 5), as was already observed in experiment AQ-2.1. Surprisingly, after the second quenching cycle and firing to 1006 ± 5 °C

pseudowollastonite crystallized in direct contact to wollastonite (Fig. 6), i.e., at a temperature that is about 120 °C below the wollastonite-pseudowollastonite transition temperature (Osborn and Schairer 1941). After stepwise heating/quenching of the sample to/from higher temperatures, pseudowollastonite continued to grow at the expense of anhydrite. Interestingly, during each cooling/quenching step most though not all pseudowollastonite grains, that were present at high temperatures, seem to be disappeared or were transformed to wollastonite.

In Fig. 5, Normalized false-color hyperspectral Raman images of the in situ experiment AQ-2.1, which were recorded at different temperatures and dwell times. The images display nucleation and isothermal growth of wollastonite at 919 ± 5 °C and the formation of α'_L-dicalcium silicate at 1093 ± 5 °C. During the cooling process, the α'_L-phase transformed to the β-phase (larnite) and remained metastable at RT. The noticeable changes in the texture between 25 ± 1 and 919 ± 5 °C result from volume changes due to mineral reactions or phase transitions, shrinkage and densification processes during firing.

In Fig. 6, at 919 ± 5 °C, wollastonite crystallized between a grain boundary of anhydrite and quartz. Pseudowollastonite could be identified at first after firing the sample to 1006 ± 5 °C and subsequent quenching. At a temperature of 1093 ± 5 °C the pseudowollastonite grains grew further and more and more wollastonite crystallized along anhydrite and quartz interfaces. Both monocalcium silicate polymorphs remained stable at RT.

3.3 In situ experiment AQ-3.1 and in situ/quench experiment AQ-3.2 (Anh + Qz, wt% 4.5:1)

Normalized false-color hyperspectral Raman images (100 μm × 100 μm) were recorded during experiment AQ-3.1 (in situ) and AQ-3.2 (in situ/quench). The anhydrite content of these samples is higher than that in AQ-2.1 and AQ-2.2. In experiment AQ-3.1, the sample was fired to 875 ± 5 °C with a heating rate of 10 °C min^{-1}. Afterwards, the sample was fired stepwise ($\sim$ 50 °C-steps) to 1137 ± 5 °C. Within the first image that was recorded at
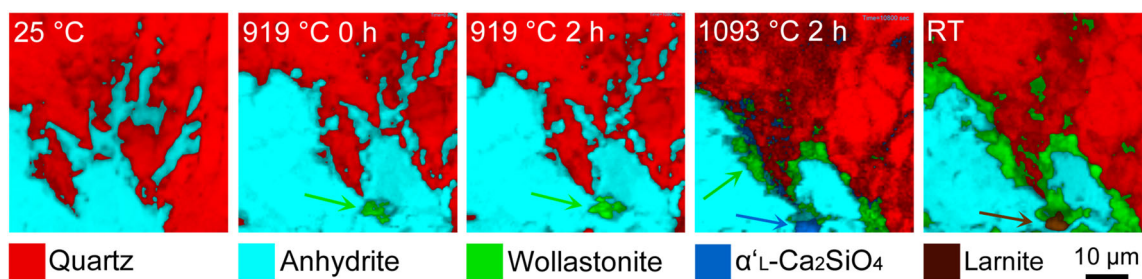
Fig. 5 Normalized false-color hyperspectral Raman images of the in situ experiment AQ-2.1
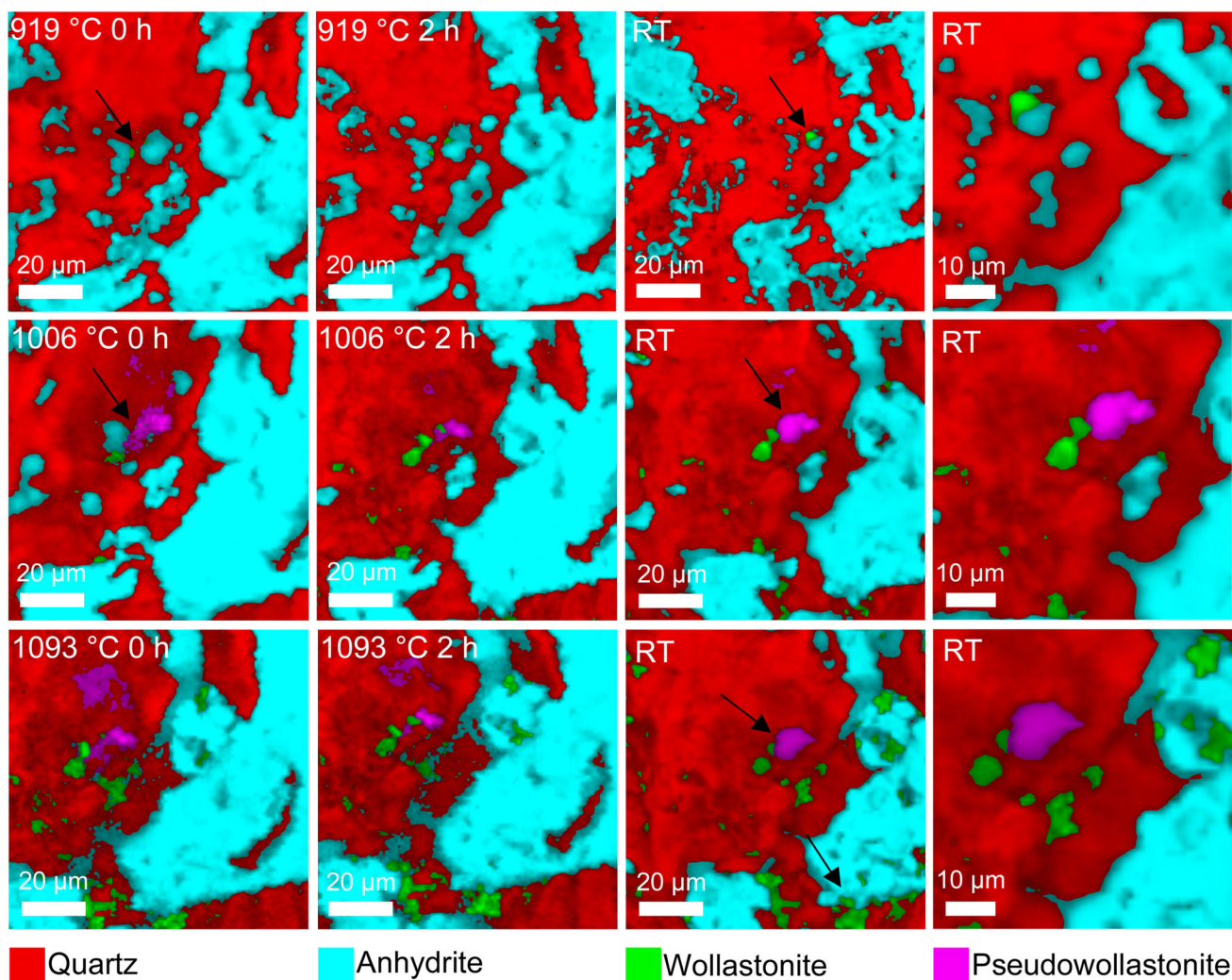
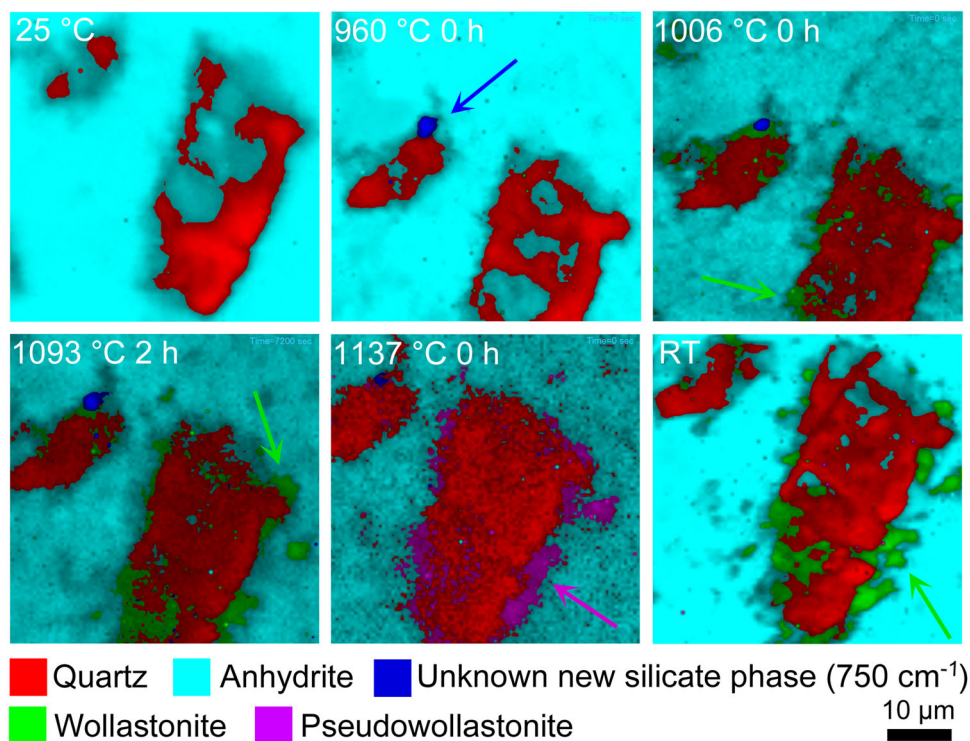**Fig. 6** Normalized false-color hyperspectral Raman images of the in situ/quench experiment AQ-2.2

971 ± 5 °C, a new but still unidentified silicate phase with the most intense Raman band near 750 cm^{-1} is located in contact to a quartz grain (Fig. 7). This phase disappeared at the expense of wollastonite during quenching to RT. Wollastonite could not be detected in situ before having fired the sample to 1006 ± 5 °C, which is nearly 100 °C above the formation temperature that was determined from the experiments with a lower anhydrite content (exp. AQ-2.1/2). At 1137 ± 5 °C, pseudowollastonite could be detected, which transformed to wollastonite during cooling to RT. The results of the in situ/quench experiment (AQ-3.2) confirm the observation that quartz is replaced by wollastonite at high temperatures. The time-series images (not shown here) revealed that wollastonite first formed near to a quartz grain after 2 h sintering at 1006 ± 5 °C. In the further course of the experiment at 1093 ± 5 °C, wollastonite increasingly crystallized at the expense of quartz (Fig. 3).

In Fig. 7, at 960 ± 5 °C, a new, not yet identified silicate phase crystallized, which disappeared after quenching the sample to RT. At 1006 ± 5 °C, wollastonite crystallized near quartz grains and seems to mainly replace anhydrite. At 1037 ± 5 °C, the high-temperature polymorph pseudowollastonite could be identified, which transformed to wollastonite during cooling to RT.

3.4 In situ experiment AQG-1 (Qz + Anh + Ge, wt%: 1:1:1)

To study the potential influence of Al on the sintering reactions in the quartz-anhydrite system, we added natural gehlenite grains to the precursor material. Gehlenite is also a common mineral phase in lignite ashes. The natural gehlenite grains were partly intergrown with grossular crystals, which is another Al source. The pressed sample was continuously fired from 25 ± 1 to 430 ± 5 °C and

Fig. 7 Normalized false-color hyperspectral Raman images of the in situ experiment AQ-3.1
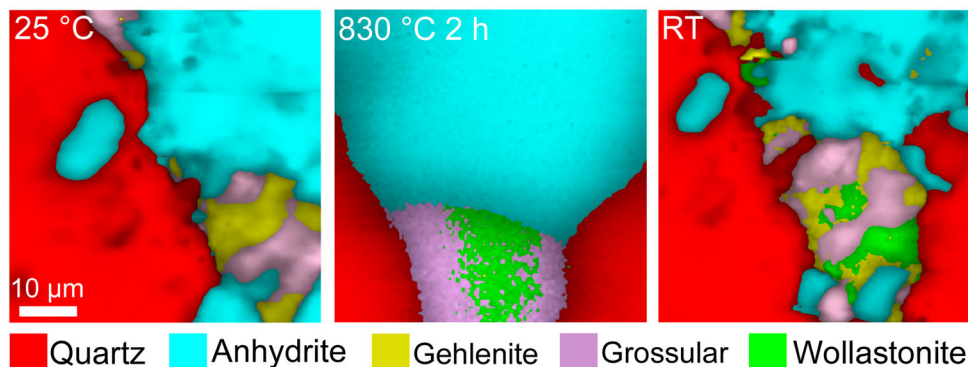
Fig. 8 Normalized false-color hyperspectral Raman images of the in situ experiment AQG-1. (Note that at 830 ± 5 °C wollastonite partly replaced gehlenite and grossular, the latter being an impurity in the natural gehlenite crystal used for the experiment.)

after having subsequently recorded three 100 μm × 100 μm-sized Raman images, the sample was fired further to 830 ± 5 °C (Fig. 1f). The first image was taken immediately after reaching the target temperature, whereas the second and third images were recorded after a dwell time of 2 and 4 h, respectively. The Raman images taken at temperatures below 430 °C did not reveal any textural or mineralogical changes. At 830 ± 5 °C and after a soaking time of about 2 h, gehlenite and grossular were partially replaced by wollastonite (Fig. 8). However, further sintering at this temperature did not cause a progress of the replacement reaction, i.e., a kind of textural equilibrium

has been reached that, however, is not a chemical equilibrium.

4 Discussion

4.1 The decomposition of anhydrite

In the binary system quartz-anhydrite, no solid-state reactions or mineral transformations could be detected below about 920 °C within dwell times of 4–6.5 h. The only spectroscopically detectable transformation was the displacive phase transition from low to high quartz at 573 °C.

The reason for this is most likely that the decomposition of pure anhydrite to lime and sulfur oxide, represented by

$$CaSO_4 \xrightarrow{T \sim 1100-1400\,°C} CaO + SO_3, \qquad (1)$$

does not start at temperatures below about 1200 °C (e.g., Hofman and Mostowitsch 1909). Other authors postulated that the β- to α-$CaSO_4$ transformation occurs at this temperature (Bensted and Varma 1971; Prieto-Taboada et al. 2014) and, based on DTA studies, suggested that the decomposition of pure anhydrite does not occur below 1400 °C (Bensted and Varma 1971; Mihara et al. 2007). However, in the present study the crystallization and the growth of wollastonite could be detected in all experiments at temperatures as low as about 920 °C. According to Gay (1965), the decomposition of anhydrite below 1100 °C is only possible within an open system. Other authors, in turn, suggested that the presence of silicate compounds may trigger the decomposition of anhydrite at lower temperatures than pure anhydrite (Mihara et al. 2007). Our results support this hypothesis. In experiments with a high proportion of quartz, wollastonite could be identified at about 920 °C, whereas in experiments with lesser quartz wollastonite first crystallized at about 1100 °C. Thus, the lower the fraction of quartz in the system, the higher the temperature at which wollastonite started to crystallize. It follows that the quartz content affects the decomposition of anhydrite and, in turn, the formation of calcium silicates as discussed in the following.

4.2 The formation of calcium silicates

It is well-known that wollastonite can be synthesized at about 1000 °C by a reaction between quartz and calcite, whereby CO_2 is released into the atmosphere and lime is formed as an intermediate product (e.g., Tschegg et al. 2009). The decomposition of anhydrite also produces lime, which is then available to react with quartz, forming a reaction rim of wollastonite around quartz grains (AQ-1, Fig. 4; AQ-2.1, Fig. 5) or replaced them (AQ-3.1, Fig. 7; AQ-3.2). This reaction can be represented by:

$$CaO + SiO_2 \xrightarrow{T \sim 1000\,°C} CaSiO_3 \qquad (2)$$
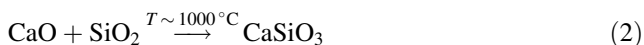
At 1125 °C, wollastonite is expected to transform to pseudowollastonite (Osborn and Schairer 1941). In experiment AQ-3.1 the sample was heated to 1137 ± 5 °C and pseudowollastonite bands could indeed be detected in the Raman spectra within the imaged area (volume). However, after quenching to RT, pseudowollastonite transformed to wollastonite. On the other hand, after the second quenching step and having fired the sample to 1006 ± 5 °C, pseudowollastonite could already be identified in direct contact to wollastonite (AQ-2.2, Fig. 6), i.e., significantly below its

stability temperature. This is at first surprising, but in agreement with observations made by Stange et al. (2018). These authors also observed the formation of pseudowollastonite already 290 °C below the phase transition temperature during sintering of a kaolin-based green body. After quenching to RT, most pseudowollastonite grains transformed to wollastonite, i.e., only a few small crystals remained metastable at RT. This is in contrast to results from experiment AQ-1. Here, both polymorphs were found as rims around quartz grains after the sample was quenched from 1093 ± 5 °C to RT (Fig. 4).

Within the ternary system anhydrite-quartz-gehlenite (exp. AQG-1), wollastonite was already detected at temperatures below 900 °C. The in situ Raman images recorded at 830 ± 5 °C clearly revealed that gehlenite and grossular were both partly replaced by wollastonite (Fig. 8). It follows that wollastonite formed by a different reaction pathway involving the decomposition of gehlenite, possibly according to following reaction:

$$Ca_2Al(AlSi)O_7 \xrightarrow{T \sim 830\,°C} CaSiO_3 + CaAl_2O_4 \qquad (3)$$
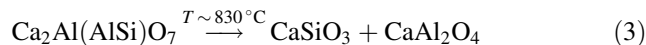
Such reaction would produce a calcium spinel ($CaAl_2O_4$), which, however, has not been detected in our experiments. Unfortunately, spinel is difficult to identify by Raman spectroscopy (Shoval et al. 2011), particular at high temperatures, and we can thus not fully rule out that a calcium spinel formed during the reaction. Alternatively, following decomposition reaction could be possible:

$$Ca_2Al(AlSi)O_7 \xrightarrow{T \sim 830\,°C} CaSiO_3 + CaO + Al_2O_3 \qquad (4)$$

However, thermodynamic calculations using FactSage 7.2 revealed that the free enthalpy of this reaction at 830 °C is about 40 kJ larger than for reaction (3). Thermodynamically, this reaction is thus less favored. In any case, whatever the details of the solid–solid replacement reaction are, a direct formation of wollastonite by the decomposition of gehlenite has so far only been described by Tschegg et al. (2009) and recently observed in situ during sintering of a kaolin-based green body (Stange et al. 2018).
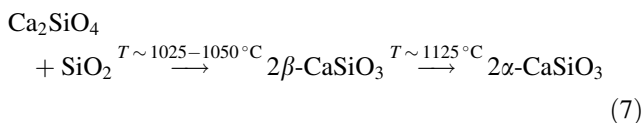
At high quartz content and sintering temperatures of 1093 ± 5 °C, dicalcium silicate was detected (AQ-2.1, Fig. 5). Like wollastonite, dicalcium silicate forms by a reaction between quartz and lime (e.g., Mitsuda et al. 1985; Singh 2006):

$$2CaO + SiO_2 \xrightarrow{T \sim 930-1020\,°C} Ca_2SiO_4 \qquad (5)$$
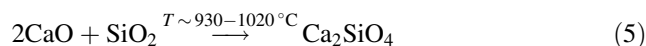
In experiment AQ-2.1, the high-temperature phase α'_L-Ca_2SiO_4 could be identified. From the time- and temperature-resolved images (Fig. 5), it is apparent that the formation of α'_L-Ca_2SiO_4 is related to the reaction between wollastonite and lime:

$$CaSiO_3 + CaO \xrightarrow{T \sim 1100\,°C} Ca_2SiO_4 \qquad (6)$$

At RT, calcio-olivine is the stable Ca$_2$SiO$_4$ polymorph (Fix et al. 1969; Sokol et al. 2015). However, Ca$_2$SiO$_4$ formed at 1093 ± 5 °C could be identified as larnite after cooling down to RT by its main fundamental Raman band near 858 cm^{-1} (Remy et al. 1997; Reynard et al. 1997). Although some authors (Fix et al. 1969; Sokol et al. 2015) claimed that β-Ca$_2$SiO$_4$ only forms during the cooling process of α'_L-Ca$_2$SiO$_4$ and transforms to γ-Ca$_2$SiO$_4$ (calico-olivine) during cooling to RT, obviously larnite remained metastable after quenching the sample from about 1100 °C to RT. The same conclusion can be drawn from the RT data of AQ-1. The Raman images show that larnite formed as reaction rim around anhydrite grains in direct contact to wollastonite, suggesting that larnite formed by reaction (6). On the other hand, rims of dicalcium silicate appear to have reacted with the adjacent quartz to wollastonite (Fig. 5). Stange et al. (2018) also observed wollastonite rims around larnite grains in a quench experiment with a calcite- and quartz-bearing kaolin green body. They referred to a study of Ptáček and co-workers (Ptáček et al. 2013), who suggested that dicalcium silicate reacts with free SiO$_2$ to wollastonite, which then converts to pseudowollastonite at temperatures above 1125 °C (Ptáček et al. 2013):

$$Ca_2SiO_4 + SiO_2 \xrightarrow{T \sim 1025-1050\,°C} 2\beta\text{-}CaSiO_3 \xrightarrow{T \sim 1125\,°C} 2\alpha\text{-}CaSiO_3 \qquad (7)$$

It follows that wollastonite cannot only form by a reaction between quartz and lime, but could also be a breakdown product of dicalcium silicate or of gehlenite if Al is present in the system. Which of the reactions is predominant in a given system seems to depend on the local chemistry. The formation of dicalcium silicate at high temperatures, for instance, is more strongly bound to anhydrite as it provides the required CaO (Rashid et al. 2014).

4.3 Quenching effects

To study the influence of quenching on the mineral paragenesis, two in situ/quench experiments with different quartz-anhydrite ratio were performed (AQ-2.2 and AQ-3.2). The in situ/quench experiment with an anhydrite-quartz weight ratio of 2:1 (AQ-2.2) showed mineral reactions other than the corresponding experiment without interim quenching cycles (AQ-2.1). During the in situ experiment (AQ-2.1) α'_L-Ca$_2$SiO$_4$ crystallized at the expense of wollastonite and transformed to larnite at RT. However, the Raman images collected during the in situ/quench experiment (AQ-2.2) do not reveal the formation of dicalcium silicate phases, indicating that a long sintering period is needed for the formation of dicalcium silicates to supply more CaO by the decomposition of anhydrite. In both experiments, the onset temperature for the first appearance of wollastonite was about 920 °C. However, in the in situ/quench experiment AQ-2.2 the crystallization of pseudowollastonite could be detected within the imaged area. Here, it was first observed after the second quenching step and after having heated the sample to 1006 ± 5 °C. Pseudowollastonite clearly grew further during the course of the heating/quenching experiment (Fig. 6), but it could not be identified during the in situ experiment AQ-2.1 (Fig. 5). It is possible that quenching triggers the formation of pseudowollastonite that grew to grain sizes larger than 10 μm in the heating/quenching experiment. Quenching seems to considerably affect the formation of pseudowollastonite in samples with an anhydrite-quartz composition of 2:1 (wt%), but had significantly less effects in the experiments with a higher anhydrite-to-quartz ratio of 4.5:1 (AQ-3.1/2). Noticeable here is that more wollastonite crystallized during the in situ run within the images area (volume). However, due to the small analyzed volume (100 μm × 100 μm × ∼ 15 μm) that cannot unconditionally be considered as being statistically representative as it contains only a relative small number of particles, any quantitative comparison of the phase composition obtained from different experiments should be rated with care.

5 Conclusion

First high-temperature, in situ Raman experiments with synthetic mixtures of natural anhydrite, quartz, and gehlenite gave new insights into solid-state calcium silicate mineral reactions:

(1) The thermal decomposition of anhydrite to CaO and SO$_3$ was found to be significantly influenced by the quartz content of the sample. In those experiments, where more quartz was available, anhydrite decomposed at lower temperatures than in experiments with lesser quartz content.

(2) Wollastonite was formed by the reaction between quartz and lime at 920 or 1000 °C depending on the quartz content. In the gehlenite bearing system, wollastonite was found to replace gehlenite at temperatures of > 830 °C. Pseudowollastonite was identified already at 1006 ± 5 °C. At about 1100 °C the crystallization of wollastonite to α'_L-Ca$_2$SiO$_4$ was observed. The formation of wollastonite by the reaction of dicalcium silicate with quartz was observed locally after cooling to RT. Accordingly,

three wollastonite-forming reactions could be identified in this study. During the cooling process, α'_L-Ca_2SiO_4 crystallized to β-Ca_2SiO_4 (larnite) and remained metastable at RT.

(3) Quenching and heating periods have a significant effect on the final sintering products.

In general, most high-temperature analyses are studied after quenching the sample to RT. However, valuable information may be lost, since quenching may change the mineralogy and new samples have to be used for each temperature–time step, making it particularly difficult to follow textural changes. Raman spectroscopy is currently the only analytical method to visualize mineral reactions in situ and two dimensions during heating or cooling with a micrometer-scale resolution. This allows the visualization of reactions among individual grains and along grain boundaries. Thus, the mechanisms of solid-state reactions can be investigated with high spatial and temporal resolution and with a high temperature accuracy ($\pm$ 5 °C). Such spatially resolved in situ studies are essential to refine current thermodynamic and kinetics models that are used to predict HT phase paragenesis or to reconstruct the temperature–time histories of naturally or technically sintered materials, e.g. in brown coal blocks. In this way, the mineral paragenesis of sintering crusts in brown coal blocks can be used as temperature indicator to unravel the actual combustion temperature of lignite. With reference to the available results, the use of quartz-rich coal leads to a premature decomposition of anhydrite and the formation of calcium silicates. It is apparent from our results that realistic modelling of HT sintering reactions has to consider the full energy landscape of a system that also includes metastable energy states.

References

Bensted J, Varma SP (1971) Infrared spectroscopic studies of calcium sulphate heated to high temperatures. Z Naturforsch 26b:690–693

Fix W, Heymann H, Heinke R (1969) Subsolidous relations in the system 2CaO·SiO$_2$–3CaO·P$_2$O$_5$. J Am Ceram Soc 52:346–347

Gay P (1965) Some crystallographic studies in the system CaSO$_4$–CaSO$_4$·2H$_2$0 I. The polymorphism of anhydrous CaSO$_4$. Mineral Mag 270:347–353

Hauke K, Kehren J, Böhme N, Zimmer S, Geisler T (2019) In situ hyperspectral Raman imaging: a new method to investigate sintering processes of ceramic material at high temperature. Appl Sci 9:1–23. https://doi.org/10.3390/app9071310

Hofman HO, Mostowitsch W (1909) The behavior of calcium sulfate at elevated temperatures with some fluxes. Trans Am Inst Min Metall Eng 32:628–653

Kostakis G (2011) Mineralogical composition of boiler fouling and slagging deposits and their relation to fly ashes: the case of Kardia power plant. J Hazard Mater 185:1012–1018. https://doi.org/10.1016/j.jhazmat.2010.10.006

Laetsch T, Downs R (2006) Software for identification and refinement of cell parameters from powder diffraction data of minerals using the RRUFF project and American Mineralogist crystal structure databases. Abstracts from 19th general meeting of the International Mineralogical Association in Kobe, Japan

Li J, Zhu M, Zhang Z, Zhang K, Shen G, Zhang D (2016) The mineralogy, morphology and sintering characteristics of ash deposits on a probe at different temperatures during combustion of blends of Zhundong lignite and a bituminous coal in a drop tube furnace. Fuel Process Technol 149:176–186. https://doi.org/10.1016/j.fuproc.2016.04.021

Li J, Zhu M, Zhang Z, Zhang K, Shen G, Zhang D (2017) Stratification and chemistry evolution of ash deposits during combustion of Zhundong lignite in a drop tube furnace. Energy Procedia 105:4216–4221. https://doi.org/10.1016/j.egypro.2017.03.904

Mihara N, Kuchar D, Kojima Y, Matsuda H (2007) Reductive decomposition of waste gypsum with SiO$_2$, Al$_2$O$_3$, and Fe$_2$O$_3$ additives. J Mater Cycles Waste Manag 1:21–26

Mitsuda T, Asami J, Matsubara Y, Toraya H (1985) Hydrothermal formation of γ-dicalcium silicate from lime-silica mixt. Cem Concr Res 15:613–621

Mohammadi H, Hafezi M, Nezafati N, Heasarki S, Nadernezhad A, Ghazanfari SMH (2014) Bioinorganics in bioactive calcium silicate ceramics for bone tissue repair: bioactivity and biological properties. J Ceram Sci Technol 5:1–12. https://doi.org/10.4416/JCST2013-00027

Nankervis JC, Furlong RB (1980) Phase changes in mineral matter of North Dakota lignites caused by heating to 1200°C. Fuel 59:425–430. https://doi.org/10.1016/0016-2361(80)90196-9

Osborn EF, Schairer JF (1941) The ternary system pseudowollastonite–akermanite–gehlenite. Am J Sci 239:715–763

Prieto-Taboada N, Gómez-Laserna O, Martínez-Arkarazo I, Olazabal MÁ, Madariaga JM (2014) Raman Spectra of the different phases in the CaSO$_4$–H$_2$O system. Anal Chem 86:10131–10137. https://doi.org/10.1021/ac501932f

Ptáček P, Opravil T, Šoukal F, Havlica J, Holešinský R (2013) Kinetics and mechanism of formation of gehlenite, Al–Si spinel and anorthite from the mixture of kaolinite and calcite. Solid State Sci 26:53–58. https://doi.org/10.1016/j.solidstatesciences.2013.09.014

Rashid AR, Shamsudin R, Hamid MAA, Jalar A (2014) Low temperature production of wollastonite from limestone and silica sand through solid-state reaction. J Asian Ceram Soc 2:77–81. https://doi.org/10.1016/j.jascer.2014.01.010

Remy C, Reynard B, Madon M (1997) Raman spectroscopic investigations of dicalcium silicate: polymorphs and high-temperature phase transformations. J Am Ceram Soc 80:413–423. https://doi.org/10.1111/j.1151-2916.1997.tb02846.x

Reynard B, Remy C, Takir F (1997) High-pressure Raman spectroscopic study of Mn₂GeO₄, Ca₂GeO₄, Ca₂SiO₄, and CaMgGeO₄ olivines. Phys Chem Miner 24:77–84. https://doi.org/10.1007/s002690050019

Shoval S, Boudeulle M, Panczer G (2011) Identification of the thermal phases in firing of kaolinite to mullite by using micro-Raman spectroscopy and curve-fitting. Opt Mater 34:404–409. https://doi.org/10.1016/j.optmat.2011.08.031

Singh NB (2006) Hydrothermal synthesis of β-dicalcium silicate (β-Ca₂SiO₄). Prog Cryst Growth Charact Mater 52:77–83. https://doi.org/10.1016/j.pcrysgrow.2006.03.011

Sokol EV, Seryotkin YV, Kokh SN, Vapnik Y, Nigmatulina EN, Goryainov SV (2015) Flamite, (Ca, Na, K)2(Si, P)O4, a new mineral from ultrahightemperature combustion metamorphic rocks, Hatrurim Basin, Negev Desert, Israel. Mineral Mag 79:583–596. https://doi.org/10.1180/minmag.2015.079.3.05

Stange K, Lenting C, Geisler T (2018) Insights into the evolution of carbonate-bearing kaolin during sintering revealed by in situ hyperspectral Raman imaging. J Am Ceram Soc 101:897–910. https://doi.org/10.1111/jace.15209

Tschegg C, Ntaflos T, Hein I (2009) Thermally triggered two-stage reaction of carbonates and clay during ceramic firing—a case study on Bronze Age Cypriot ceramics. Appl Clay Sci 43:69–78. https://doi.org/10.1016/j.clay.2008.07.029

Vuthaluru HB, Zhang DK (2001) Effect of Ca- and Mg-bearing minerals on particle agglomeration defluidization during fluidized-bed combustion of a South Australian lignite. Fuel Process Technol 69:13–27. https://doi.org/10.1016/S0378-3820(00)00129-6